ORIGINAL ARTICLE

Fabrication of submillimetre structures on pure titanium by non-aqueous electrolyte jet machining

Cheng Guo[1,2] · Xiao Du[1,2] · Jingwen He[1,2] · Weizhen Zhuang[1,2] · Bin Xu[1,2]

Abstract

Titanium and its alloys are widely utilized in the field of aerospace and medical devices, owing to their impressive high-temperature durability and excellent corrosion resistance. Many researchers have machined millimeter-scale features on titanium using electrochemical jet machining (EJM). However, achieving submillimetre scale features on titanium with high efficiency and surface integrity is still a hindrance. In this research, a small nozzle with a diameter of 200 μm has been proposed for EJM of pure titanium (TA2) with NaCl-ethylene glycol (EG) solution. This non-aqueous electrolyte is able to prevent the formation of oxide layers during the machining process. In the experimental part, the utilization of EJM in processing dimples and channels on TA2 has been examined. The direct current mode and the pulsed current mode have been compared in terms of dimensions, surface finish, and material removal localization. It is found that by utilizing suitable parameters, EJM with non-aqueous electrolyte is suitable to manufacture submillimetre structures on pure titanium with high precision and high surface quality.

Keywords Electrochemical jet machining · Non-aqueous electrolyte · TA2 · Submillimetre structures

1 Introduction

Due to its advantageous mechanical properties and compatibility with living organisms, titanium has gained widespread application in the fields of aerospace engineering [1] and biomedical sciences [2]. In these fields, it is common for components to require precise submillimetre features, which involves various demands regarding shape and dimensions. However, the traditional mechanical techniques employed for machining these intricate features on titanium encounter various challenges, including high cutting tool wear, subpar machining precision, and limited machining size [3]. At present, there has been research conducted on non-traditional energy-based techniques, including laser beam machining (LBM), ultrasonic machining (USM), and electrical discharge machining (EDM), because of their potential to improve machining accuracy and decrease tool wear. Sarilov et al. [4] point out that EDM of titanium alloys requires precise electrical parameter control to avoid machining defects such as surface cracks or excessive heat-affected zones. In addition, the wear rate of the EDM tool electrode is too fast, and the electrode needs to be replaced frequently, increasing the cost and machining time. Hung et al. [5] employed femtosecond laser microfabrication to produce an accurately dimensioned biliary stent made of nickel-titanium alloy. By using this laser technique, regulating heat transfer and achieving the smallest possible thermal area are possible. However, it should be noted that the femtosecond laser system carries a hefty price tag [6].

Electrochemical machining (ECM) is a controllable anodic electrochemical dissolution process used for shaping components in an electrolytic cell. ECM involves the use of an electrically conductive tool, known as the cathode, and an electrolyte solution to selectively remove material from the workpiece, acting as the anode. This process enables precise and intricate shaping of various difficult-to-cut metals and alloys, by utilizing specific electrochemical

✉ Cheng Guo
cheng.guo@szu.edu.cn

1 Guangdong Provincial Key Laboratory of Micro/Nano Optomechatronics Engineering, College of Mechatronics and Control Engineering, Shenzhen University, Shenzhen 518060, China

2 Shenzhen Key Laboratory of High Performance Nontraditional Manufacturing, College of Mechatronics and Control Engineering, Shenzhen University, Shenzhen 518060, China

reactions. ECM of titanium alloy has no mechanical stress and thermal influence and can process high precision and complex shape, which has been proven to be an efficient titanium alloy processing technology [7]. Over the past few years, a multitude of researchers have dedicated their efforts to investigating the application of ECM of titanium alloys. This particular research area has gained significant attention due to the unique properties and challenges associated with titanium alloys. Qu et al. [8] examined the viability of employing axial electrolyte flushing in wire electrochemical machining (WECM) of TC1 titanium alloy. Klocke et al. [9] conducted a foundational study on the electrochemical machinability of specifically chosen modern titanium and nickel alloys in aviation engine parts. ECM, in comparison to milling and electrical discharge machining techniques, yielded the highest material removal rate and provided the best surface quality. Wang et al. [10] investigated the use of a sheet-shaped cathode to improve the uniformity of deep and narrow channels produced by ECM on TB6 titanium alloy. Liu et al. [11] conducted a study of ECM on TB6 titanium alloy in $NaNO_3$ solution. The extensive exploration and investigation of ECM for titanium alloy machining have resulted in advancements in tool design, electrolyte selection, process parameters optimization, and monitoring techniques.

As a significant variation of ECM, electrolytic jet machining (EJM) utilizes an electrolyte column as a cathode tool to strike the workpiece through a nozzle and dissolve the anode to remove the workpiece material. Compared to traditional ECM, EJM provides a simplified tool structure and greater flexibility, enabling the machining of channels, planes, or other complex structures with numerical control [12]. The simplified EJM tool structure also makes machining operations more precise and efficient, resulting in improved accuracy and surface finish [13]. Moreover, EJM has significant advantages in surface structuring of hard-to-cut materials such as titanium alloys and nickel-based superalloys because it is free of tool wear, thermal and residual stress, as well as cracks and burrs. Many scholars have made great efforts in the research on EJM of titanium alloys. Hackert et al. [14] utilized a tubular electrode with the inner diameter of 0.1 mm to generate intricate micro-surface structures on stainless steel surfaces. Schubert et al. [15] employed pipe electrodes, measuring 0.1 mm in inner diameter, to intricately shape three-dimensional surfaces on stainless steel, resulting in sharp edges. Kai et al. [16] conducted experimental research on ECM cutting of metal plates. They discovered that EJM is capable of precisely cutting stainless steel plates with a thickness of 3 mm. Kawanaka et al. [17] conducted a study on the surface quality after EJM, and their findings indicate that higher current density contributes to achieving a mirror-like surface. Speidel et al. [18] investigated the effects of different innovative electrolytes on the

EJM of TC4 titanium alloy, laying the groundwork for further understanding. Wang et al. [19] utilized a novel cathode tool with a negative incident angle to carry out EJM on TC4 titanium alloy. Their study aimed to investigate the impact of various jet angles on the distribution of flow field, surface quality, material removal rate, width of the flat-bottom area, processing depth, and taper. Liu et al. [20] successfully achieved millimeter-scale features on Ti1023 titanium alloy through EJM. However, achieving more precise structures on the surface of titanium alloys remains a challenge in the field of EJM. Higher precision implies new applications and improved performance of titanium alloy components in industries.

Thus, in this research, a nozzle with a submillimetre scale (200 μm) was utilized as the cathode for EJM, with a 1 mol/L NaCl-ethylene glycol (EG) solution serving as the electrolyte for electrochemical reactions. The aim was to examine and analyze the influence of this submillimetre size nozzle on the processing of the TA2 surface, in terms of typical dimple and channel features. Through the analysis of the surface topography and depth cloud map of TA2 samples after EJM, it has been demonstrated that the miniature nozzle allows for submillimeter scale machining on TA2. Furthermore, the study also examined the effect of waveforms (direct current and pulsed current) on the machining performance, as well as the impact of nozzle movement speed on channel processing. Through the research, it is found that the dimple machining performance is best when the direct current is used and the voltage is set to 140 V, and the channel machining performance is best when the voltage is 100 V and the nozzle scan rate is set to 20 μm/s.

2 Experiments

2.1 Materials and equipment

The experimental workpiece material is TA2, specifically an industrial-grade pure titanium with a sole α phase. The TA2 surface to be machined has been polished with #5000 sandpaper. Figure 1 displays a micrograph and the size distribution of TA2 grains, which were obtained through electron back scatter diffraction (EBSD) analysis. The electrolyte used for electrochemical reactions is a 1 mol/L NaCl-EG solution. Since it has been verified that NaCl-EG solution can effectively eliminate the oxide layer on titanium during the electrochemical polishing process [21], employing this solution for fabrication of submillimetre structures on TA2 may enhance precision and surface quality. The experimental setup used in the lab is a CNC platform for EJM, as shown in Fig. 2. Scanning electron microscope (SEM) was used to observe the overall concave shape and stray corrosion of the dimples and channels. Laser scanning confocal microscope

Fig. 1 **a** EBSD micrograph of TA2; **b** grain size distribution
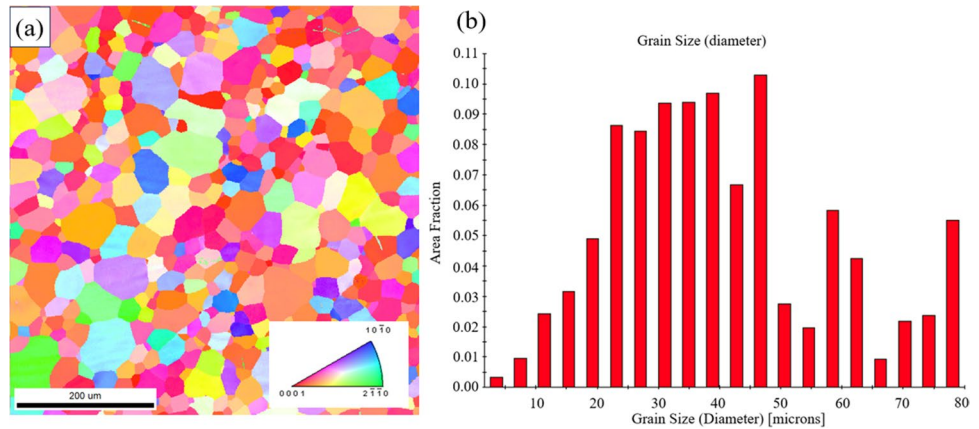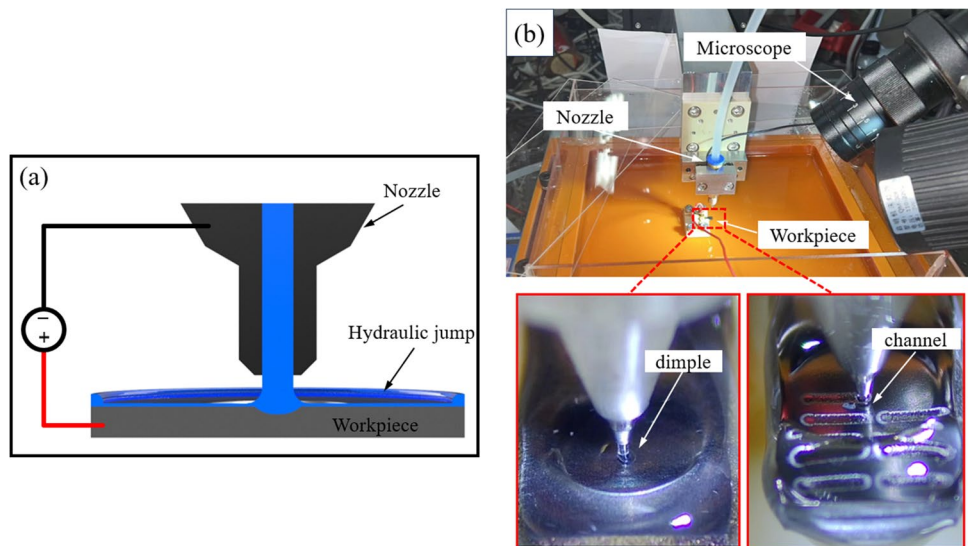

Fig. 2 Experimental device schematic and physical pictures: **a** Illustration of EJM principle; **b** EJM experimental device diagram

(LSCM) was used to analyze the three-dimensional (3D) and cross-sectional profiles.

2.2 Experimental procedure

NaCl-EG electrolyte is continuously injected from the nozzle to the surface of the workpiece during machining. A voltage is applied between the nozzle and the workpiece to locally dissolve the workpiece material. Due to the localization of the process current density, the dissolution of the anode is limited to the exposed surface directly below the electrolyte. This phenomenon is realized by the action of the hydraulic jump phenomenon. Specifically, when the fast-flowing electrolyte hits the surface of the workpiece, a thin fast-flowing electrolyte film is formed beneath the nozzle. Subsequently, the thickness of the electrolyte in the region away from the nozzle suddenly increases to a subcritical state. With the help of this fast and thin electrolyte layer, the current density is to a great extent concentrated [22].

The main electrochemical reactions that occur during electrolysis are

$$Ti \rightarrow Ti^{4+} + 4e^- \tag{1}$$

$$Ti^{4+} + 4Cl^- \rightarrow TiCl_4 \tag{2}$$

Experiments have been conducted using the setup shown in Fig. 2, where the workpiece was fixed underneath the nozzle and the control system was used to manipulate the nozzles on the machine to ensure that the nozzles were accurately placed directly above the specified location of the workpiece. The inter-electrode gap (IEG) between the nozzle and the workpiece is set to 200 μm. The nozzle inner diameter is 200 μm, and the electrolyte flow rate is set to 51 mL/min. In order to study the feasibility of machining submillimetre structures on TA2 with NaCl-EG solution, dimples and channels have been experimentally fabricated on TA2 separately. In order to compare the effects of the direct current and the pulsed current, a self-defined parameter,

effective voltage time (t_{effv}) has been used to represent the actual processing time. In the direct current experiments, t_{effv} indicates the dwell time (t_{dwell}). In the pulsed current experiments, the pulse parameters are expressed as pulse cycle (t_{cycle}) and pulse width (t_{on}), and $t_{effv} = t_{dwell} \times \lambda$ ($\lambda = t_{on}/t_{cycle}$, i.e., duty ratio).

3 Results and discussion

3.1 EJM of submillimetre dimples

3.1.1 EJM of dimples with direct current

Figure 3 illustrates the depth and diameter of the dimple obtained by varying the voltage from 60 to 140 V, under the condition of the t_{effv} of 5 s. Figure 4 depicts the line graph of changes in the diameter and depth of dimples. As can be seen in Fig. 4, at the voltage of 60 V, the diameter of the dimple is about 198 μm and the depth is only about 5 μm. When the voltage reaches 140 V, the diameter of the dimple increases to around 346 μm and the depth increases to around 24 μm. At the voltage of 60 V, it was observed that almost no dimples are formed in Fig. 3a, while extensive scattered corrosion occurred on the TA2 directly beneath the nozzle. This is due to the fact that the low voltage results in a low current density during machining, affecting both the material removal efficiency and the surface finish of the dimple. By examining the line graph (Fig. 4), it is evident that with the increase in voltage, both the diameter and depth of the dimples gradually expand. This is due to an increase
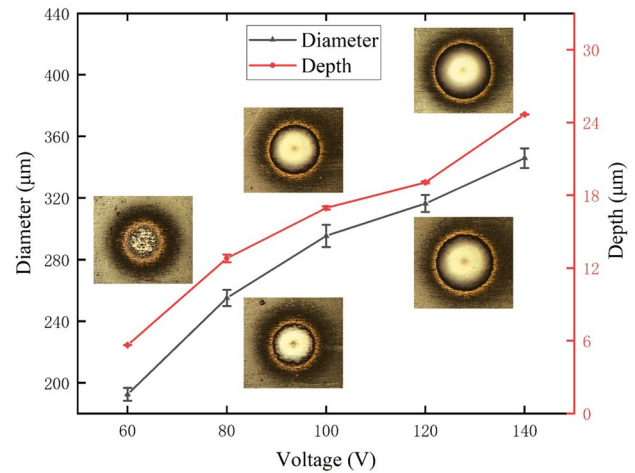

Fig. 4 Diameter and depth of the dimples under different voltages at the t_{effv} of 5 s

in current density, which leads to an increase in material removal. The increased current density enhances the overall efficiency of current flow, as more electrons are effectively utilized in the electrolysis process. As the voltage increases, the rate of electrochemical reactions between the electrolyte and the surface of the workpiece accelerates, leading to a faster removal rate of material and consequently an expansion in the depth of the dimples. Furthermore, with the increase in current density, the range of electrolytic action will likewise widen, resulting in an enlargement in the diameter of the dimples. It can be seen from the SEM image (Fig. 3) that the indicated roughness of the crater decreases
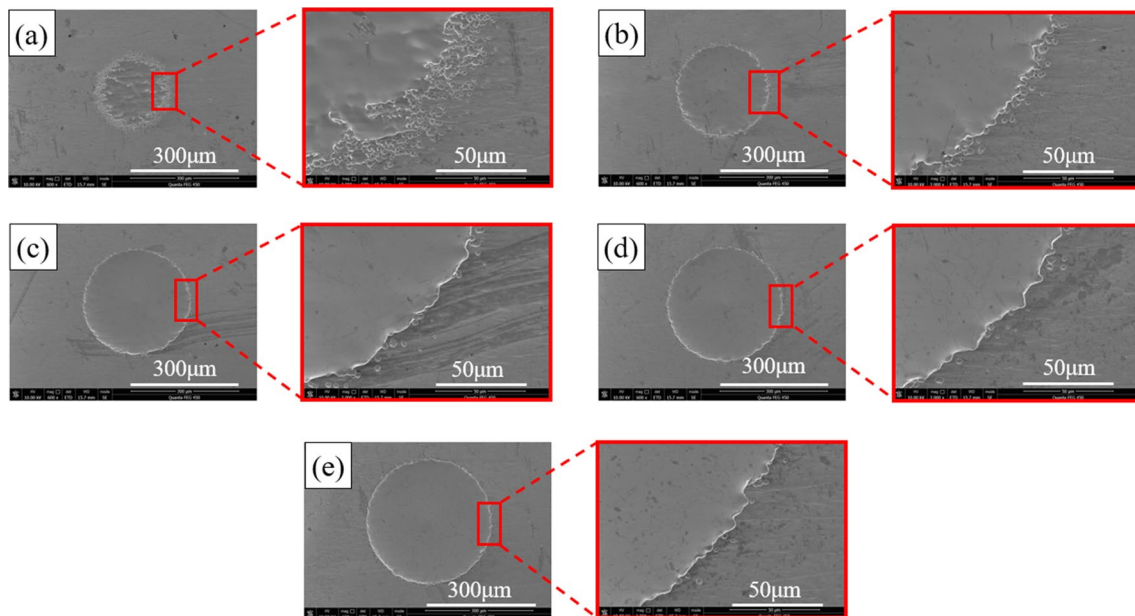

Fig. 3 SEM images of dimples under different voltages at the t_{effv} of 5 s: **a** 60 V; **b** 80 V; **c** 100 V; **d** 120 V; **e** 140 V

as the voltage increases and no evident pit corrosions occur at the edges of the dimples. This can probably be attributed to the jet shape and the characteristic of the NaCl-EG electrolyte. With the increase in voltage, the NaCl-EG electrolyte not only ensures a high level of surface cleanliness but also enhances the efficiency of material removal. These changes can be attributed to factors such as enhanced ion diffusion and modified charge transfer rates.

Figure 5 exhibits the SEM image of the dimples under the t_{effv} of 10 s. Figure 6 shows the depth cloud map of the dimple. As can be seen in Fig. 6, when the voltage is 60 V, the diameter of the dimple is about 269 μm and the depth is about 22 μm. Compared to the case with the t_{effv} of 5 s

in Fig. 3a, sharp edges can be obtained. It indicates that the scattered corrosion in Fig. 3a is a transitional process if the t_{effv} is extended. When the voltage reaches 120 V, the diameter of the dimple increases to around 366 μm and the depth increases to 42 μm. From the graph (Fig. 5), it is evident that the dimples obtained through processing with the t_{effv} of 10 s exhibit similar surface smoothness compared to those obtained with the t_{effv} of 5 s. This suggests that longer t_{effv} is not a key factor that influence surface roughness if the dimple forms steadily. Nevertheless, if the t_{effv} is prolonged, it could potentially lead to a degradation in the shape of the dimple due to an excessive reaction between the electrolyte and the dimple walls that causes
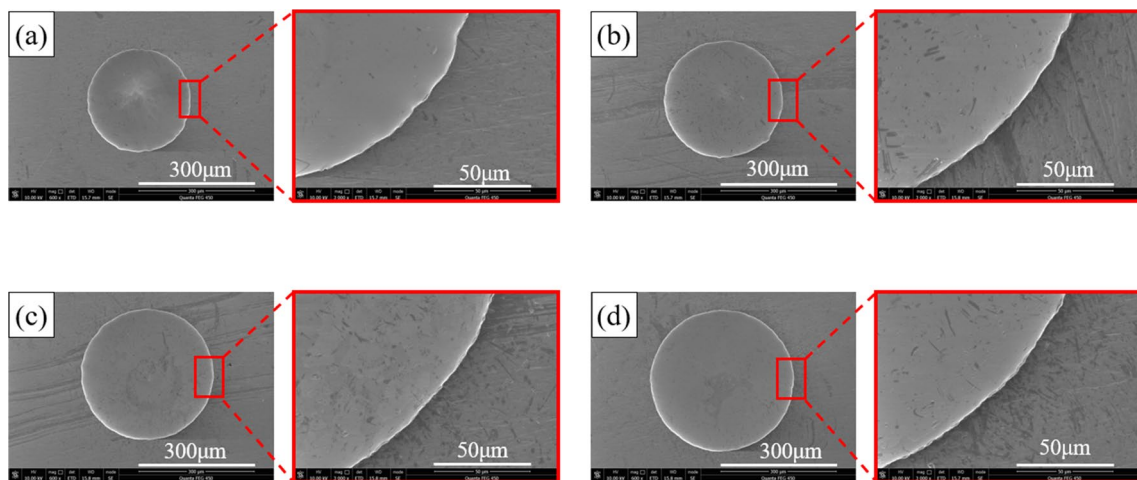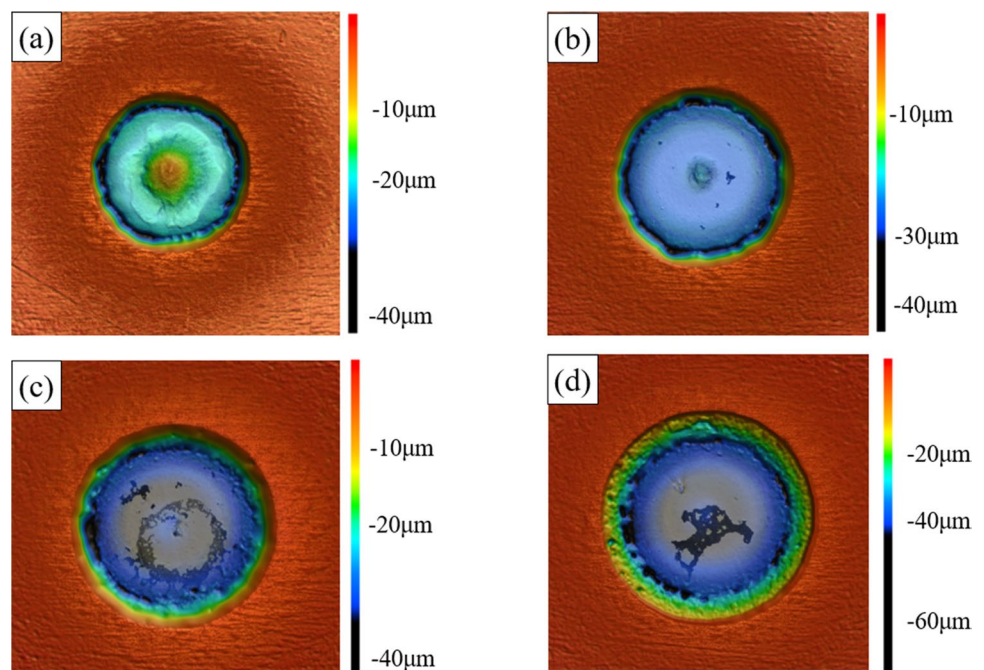

Fig. 5 SEM images of dimples at different voltages with the t_{effv} of 10 s: **a** 60 V; **b** 80 V; **c** 100 V; **d** 120 V

Fig. 6 Depth cloud map of dimples at different voltages with the t_{effv} of 10 s. **a** 60 V; **b** 80 V; **c** 100 V; **d** 120 V

uneven material removal and damage to the integrity of the dimple walls.

3.1.2 EJM of dimples with pulsed current

Many research results have demonstrated that the use of pulsed current can significantly enhance the machining performance of ECM. Therefore, EJM experiments with the pulsed current have been conducted, and two groups of experiments have been carried out with different duty ratios, while keeping other parameters constant. Figure 7 presents the SEM images showcasing the utilization of pulsed electrical currents for the dimple fabrication. The frequency of the pulsed current is 5 kHz, with a duty ratio

of 0.5. Figure 8 presents the depth cloud map illustrating the machined dimples with varying the duty ratio from 0.2 to 0.5. When the duty ratio is 0.2, the morphology of the dimples change with the t_{effv}. When the t_{effv} is 5 s, the depth of the dimple is about 21 μm. When the t_{effv} is 10 s, the depth of the dimple increases to around 40 μm. When the t_{effv} is 15 s, the depth of the dimple increases to around 57 μm. However, the surface quality changed evidently. When the duty ratio is set to 0.5 and the t_{effv} is 15 s, the depth of the dimple increases to around 44 μm and the bottom surface quality is improved. From the depth cloud graph (Fig. 8), it is evident that the depth achieved by using pulsed current for EJM of TA2 dimples is greater compared to using direct current. This increased depth is
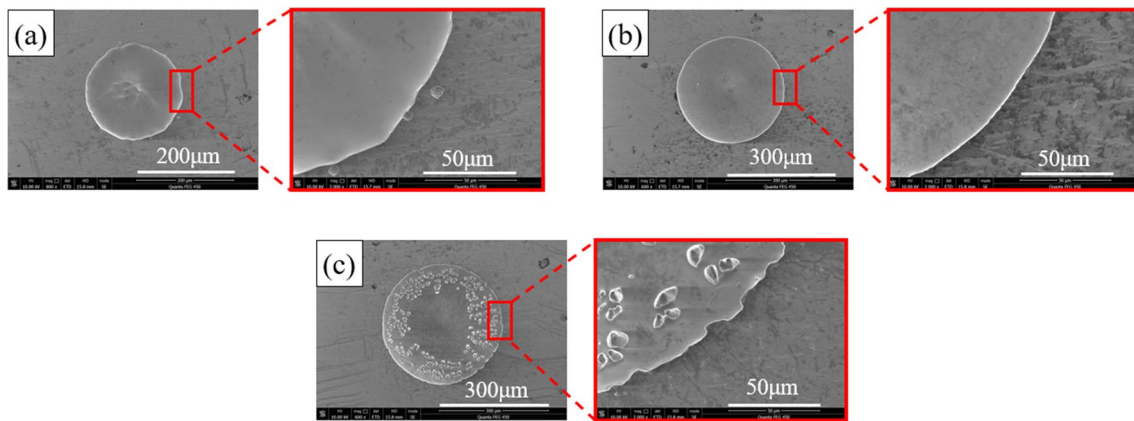

Fig. 7 SEM images of dimples under different t_{effv} with the pulsed current of 0.5 duty ratio: **a** 5 s; **b** 10 s; **c** 15 s
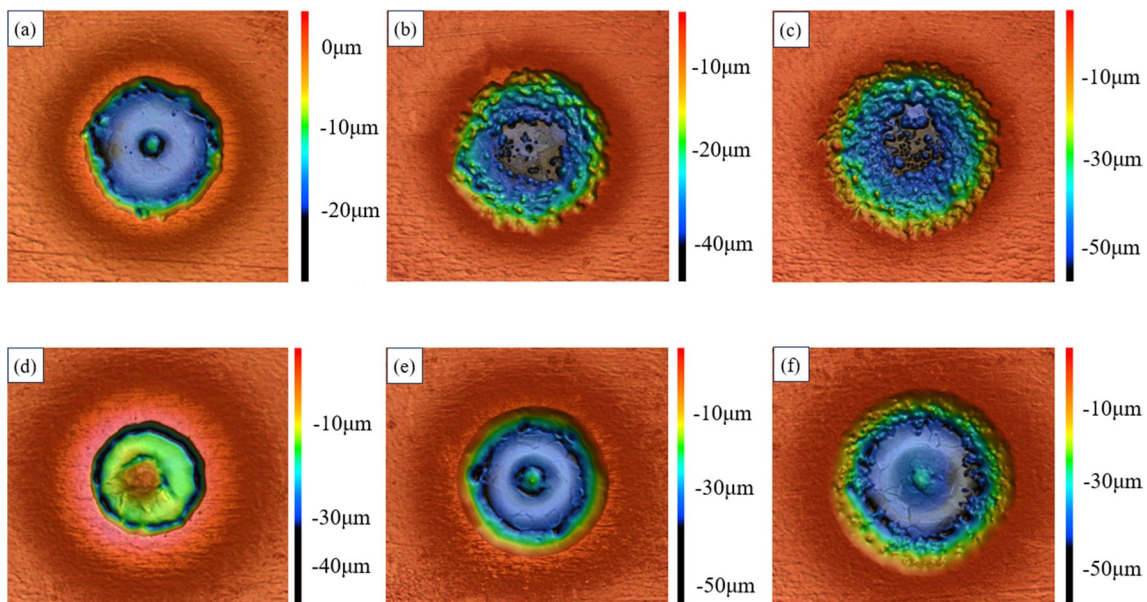

Fig. 8 The depth cloud map of dimples with different t_{effv} under pulsed current; **a**, **b**, and **c** are with the duty ratio of 0.2 and with the t_{effv} of 5 s,10 s, and 15 s, respectively; **d**, **e**, and **f** are with the duty ratio of 0.5 and the t_{effv} of 5 s,10 s, and 15 s, respectively

attributed to the unique characteristics of pulsed current, which allows for concentration of electrical energy during the EJM process. Figure 9 illustrates the possible chemicals generated on the surface of TA2 during processing. The surface roughness of the dimples is influenced by the formation of oversaturated thin film during the electrochemical process (Fig. 9). Studies conducted by Rosenkranz et al. [23] have highlighted that the existence of oversaturated thin film throughout the entire processing contributes to enhancing the surface smoothness of the dimples. Conversely, if the oversaturated thin film is penetrated, it will cause deterioration in surface roughness. It can be observed from Fig. 8 that the application of pulsed current in dimple machining leads to the formation of numerous protrusions on the dimple surface, resulting in a significantly diminished surface smoothness. It is likely that the presence of a surface with an oversaturated polishing film, characterized by a water gradient, is caused by the pulsed current being in the on state. Nevertheless, in the pulsed current mode, the thickness of the oversaturated film is determined by the current density and the pulse on duration, i.e., t_{on}. When the current is in the off state (t_{off}), a continuous oversaturated film fails to form due to diffusion, leading to the film not adhering to the surface and thereby producing a rough surface. As shown in Fig. 8a–c, with the depth growing, the current density becomes low, which hinders the continuous oversaturated film formation and degrades the surface quality.

As the duty ratio fluctuates, the machining surface of the dimple also undergoes evident variations. With changes in the duty ratio, there are alterations in the electrolytic product ejection and heat generation during the machining process, leading to conspicuous transformations in the surface properties of the dimple. These disparities can be observed as modifications in surface roughness, microstructural features, and even the completeness of the machined dimple.

3.2 EJM of submillimetre channels

Due to the flexibility of EJM, it allows for the processing of more intricate shapes on TA2. To investigate the feasibility of using EJM to process submillimetre concave channels on TA2, the experiments involve different nozzle scanning rates and different current modes. The nozzle travels along a straight path to examine the formation of the channel on TA2 material. When using direct current to fabricate channels, the nozzle scanning rate is set to 0.05 mm/s.

3.2.1 EJM of channels with direct current

Figure 10 shows the SEM images of the channels processed at the voltages of 60 V and 140 V. Figure 11 displays the depth cloud maps and surface roughness of channels machined using direct current at different voltages. From the graph (Fig. 11), it is clear that when the voltage reaches 60 V, the surface of the channel becomes extremely rough, with the surface roughness reaching 0.468 µm. Figure 10a also verifies this point. As the voltage increases, the width and depth of the channels increase synchronously, and the surface roughness of the channels exhibits a decreasing trend. Figure 10b exhibits the SEM picture at the voltage of 140 V. Shape edges and uniform microstructures can be observed with high surface integrities. Even grains can be figured out due to different corrosion rates in different crystal orientations. Figure 12 shows the histogram of the width and depth of the channels. As can be seen from Fig. 12, when the voltage is 60 V, the depth of the channel is around 7 µm and the width is around 130 µm. When the voltage is set to 140 V, the depth of the channel increases to around 26 µm and the width increases to around 300 µm. It can be seen that

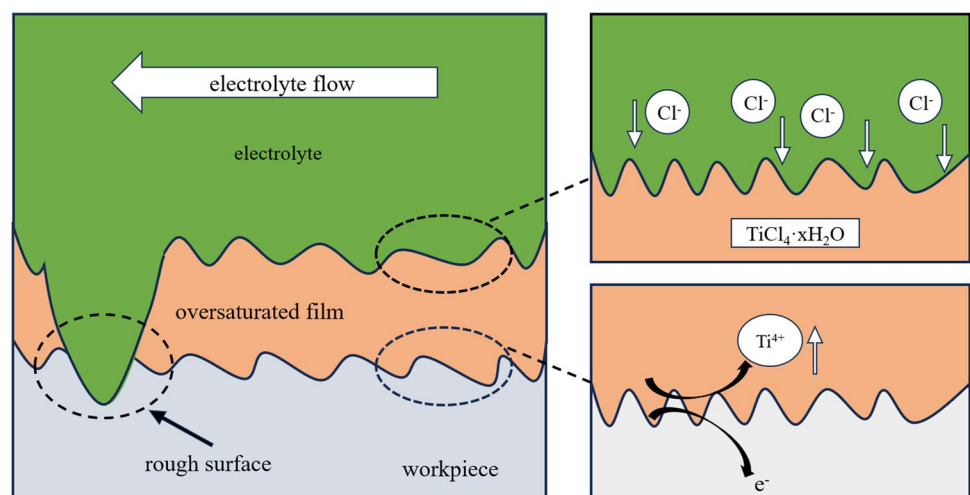**Fig. 9** Chemicals produced on the surface of TA2 during the EJM process

Fig. 10 SEM images of channels with a scanning rate of 0.05 mm/s at different voltages: **a** 60 V; **b** 140 V
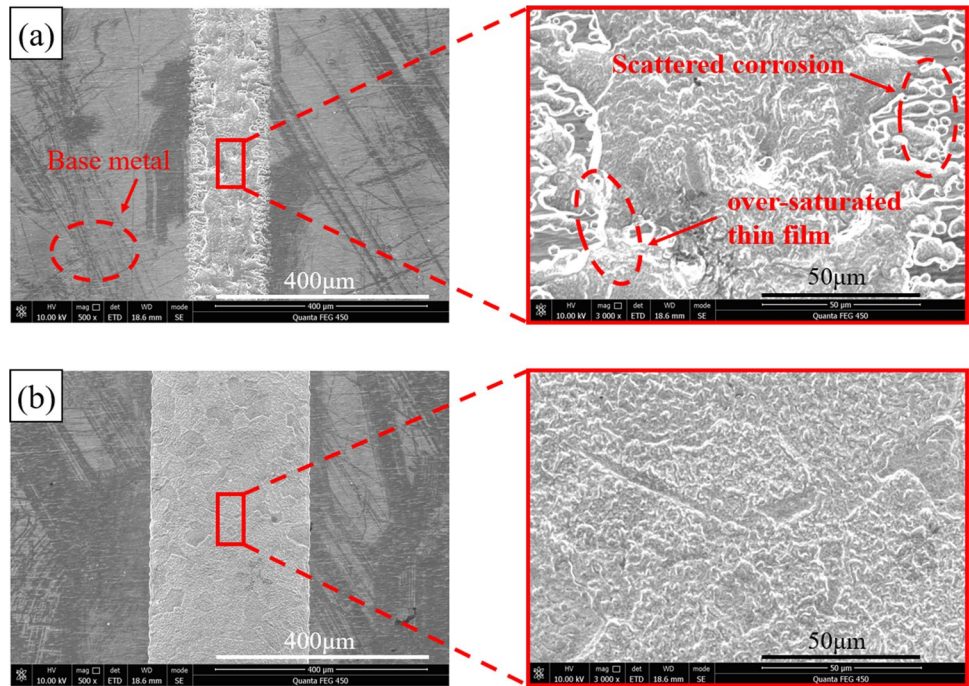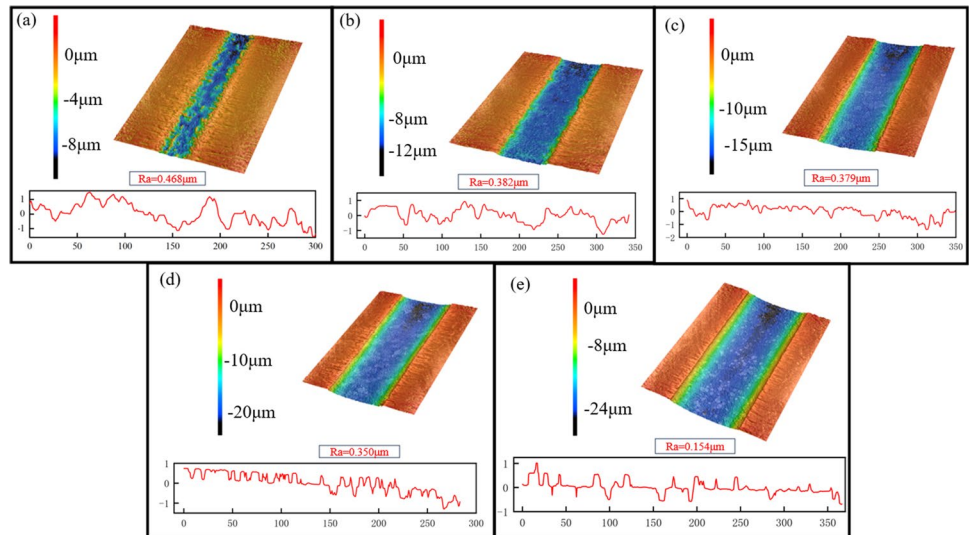

Fig. 11 Depth cloud maps of channels with a scanning rate of 0.05 mm/s at different voltages: **a** 60 V; **b** 80 V; **c** 100 V; **d** 120 V; **e** 140 V

the width and depth of channels have undergone above 50% adjustments, which indicates that adjusting the voltage is an efficient way to adjust the profile of the channels.

In order to investigate the effect of the nozzle scanning rate on EJM machining of TA2 channel under the direct current, the voltage is set to 100 V and the nozzle scanning rate is varied from 0.02 to 0.07 mm/s in this experiment. Figure 13 shows the SEM images of channels at the nozzle scanning rate of 0.02 mm/s and 0.07 mm/s. It can be observed that the scanning rate of 0.07 mm/s leads to a better surface integrity without protrusions. This is related to the exposure time to low current densities. In another way, the

nozzle scanning rate of 0.02 mm/s brings more exposure time to low current densities, and the thick oversaturated film fails to form on the machined surface. Figure 14 displays the depth cloud map and surface roughness of channels. From Fig. 14, it can be seen that as the scanning rate increases, the surface roughness at the bottom of the channels generally decreases. When the scanning rate is 0.02 mm/s, the roughness of the channel bottom along the nozzle moving direction is 0.432 μm. When the scanning rate is 0.07 mm/s, the roughness value is 0.155 μm. Figure 15 shows the cross-sectional view of channels. It can be observed that as the scanning rate increases, both the width and depth of the
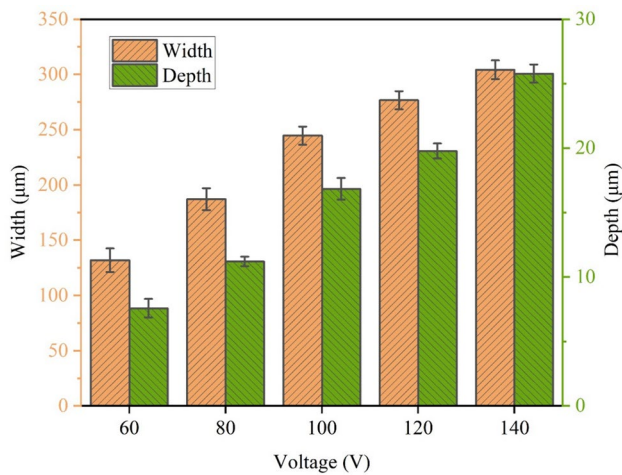
Fig. 12 Histogram of width and depth of channels with scanning rate of 0.05 mm/s at different voltages

channels decrease (Fig. 15). Figure 16 presents the width and depth values. When the scanning rate is 0.02 mm/s, the depth of the channel is about 60 μm, and the width is about 365 μm. When the scanning rate is 0.07 mm/s, the depth of the channel decreases to around 17 μm, and the width decreases to around 295 μm.

3.2.2 EJM of channels with pulsed current

The duty ratio of the pulse current is set to 0.5, and the frequency is set to 5 kHz. Figure 17 shows the SEM images

of the channels processed at different scanning rates. The similar trend can be noticed, and evident protrusions can be found when the scanning rate is 0.02 mm/s. Figure 18 shows the depth cloud maps and surface roughness of channels under the pulsed current. The variation of the surface roughness of the channels under pulsed condition is similar to that under the direct current condition. The roughness at the bottom along the nozzle moving direction is maximum (0.472 μm) when the scanning rate is 0.02 mm/s, while that is minimum (0.298 μm) when the scanning rate is 0.07 mm/s. Figure 19 shows the cross-sectional views of channels at different scanning rates, which demonstrates narrow channels compared with the direct current case. Figure 20 depicts the histogram of width and depth of channels. The scanning rate has a significant impact on the depth variation of channels, while the width varies little. At the scanning rate of 0.02 mm/s, the depth of the channel is about 35 μm and the width is about 250 μm. At the scanning rate of 0.03 mm/s, the depth of the channel decreases to around 25 μm and the width decreases to around 243 μm. While at the scanning rate of 0.07 mm/s, the depth of the channel decreases to around 9 μm and the width decreases to around 180 μm. Since the nozzle diameter remains constant at 200 μm, the width of the channel is even smaller than the nozzle diameter. As shown in Fig. 19, the cross-sectional views of channels, the width, and depth of channels increase with the increase in the scanning rate. Comparing to the cross-sectional views of the direct current case with the similar depth (Fig. 15), channels have smaller width and sharper edges, indicating better material removal localization. In

Fig. 13 SEM images of channels at different scanning rates with a voltage of 100 V: **a** 0.02 mm/s; **b** 0.07 mm/s
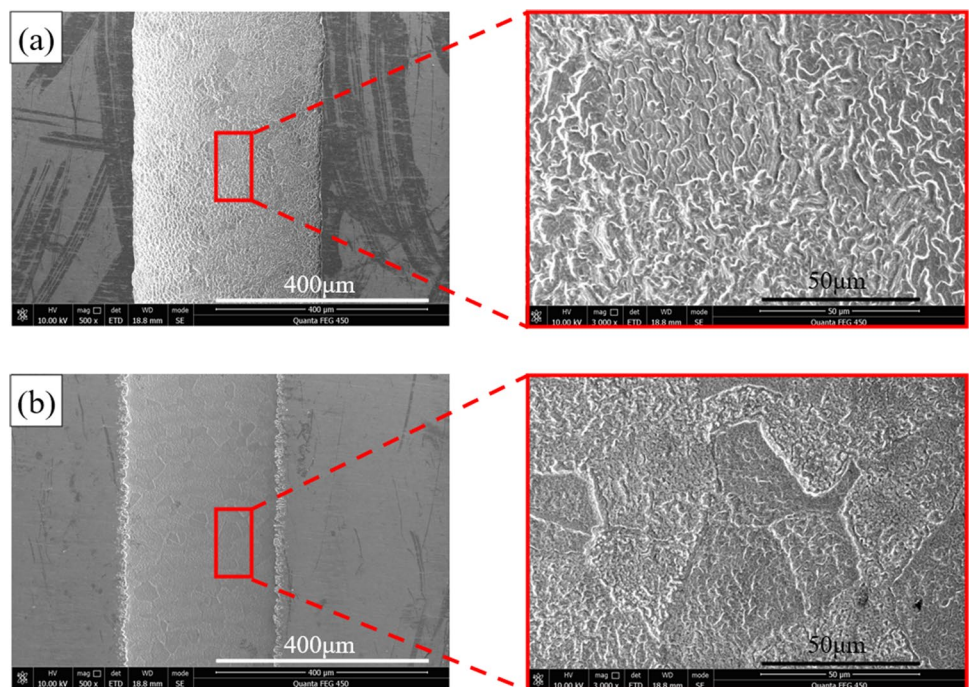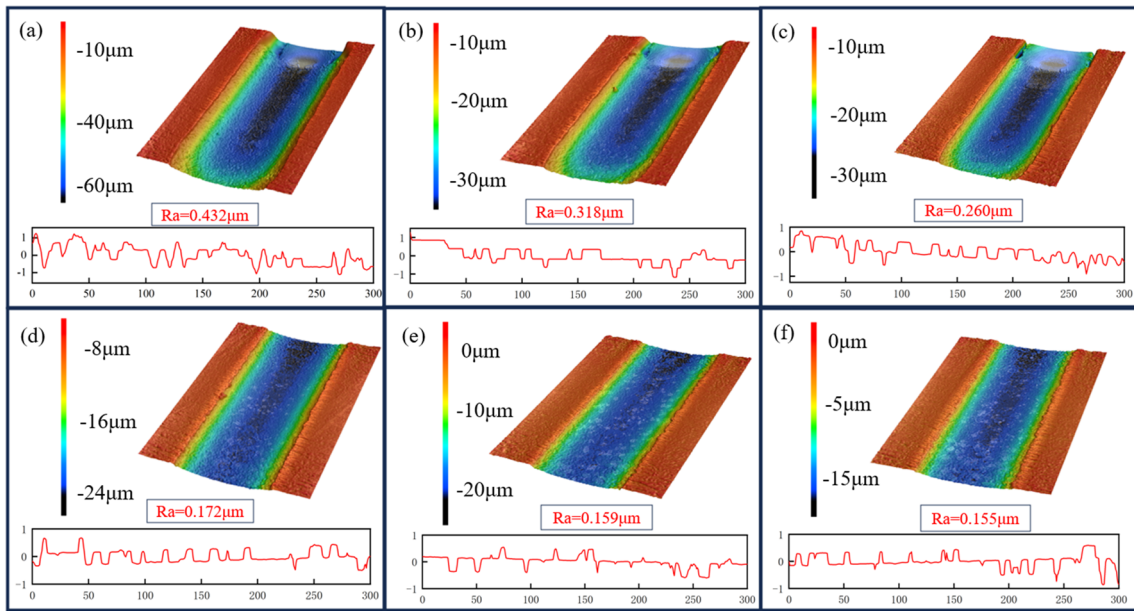
Fig. 14 Depth cloud maps of channels at different scanning rates with the voltage of 100 V: **a** 0.02 mm/s; **b** 0.03 mm/s; **c** 0.04 mm/s; **d** 0.05 mm/s; **e** 0.06 mm/s; **f** 0.07 mm/s
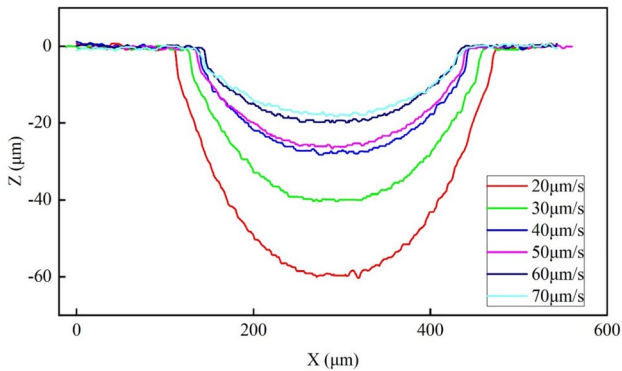

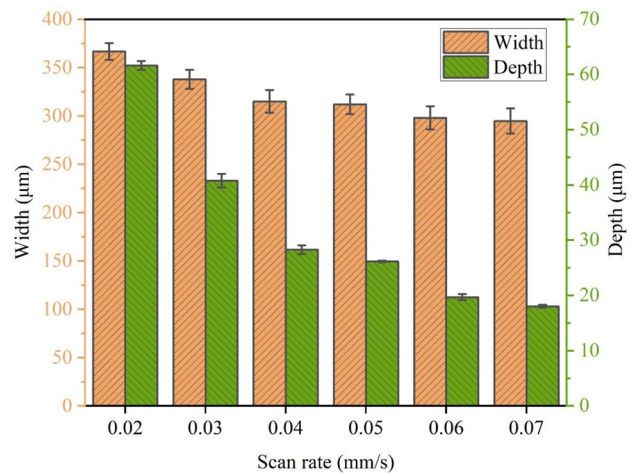**Fig. 15** Cross-sectional views of channels at different scanning rates with the voltage of 100 V

Fig. 16 Histogram of width and depth of channels at different scanning rates with the voltage of 100 V

addition, when compared to the direct current case, the pulsed current counterparts exhibit bigger surface roughness along the nozzle moving direction.

4 Conclusions

In this study, fabrication of submillimetre structures on TA2, a kind of pure titanium, has been realized by electrolytic jet machining (EJM) technology with non-aqueous organic electrolyte, NaCl-ethylene glycol (EG) solution, which avoid to create passivation films on the workpiece surface in water-based salt electrolytes. By employing a small-size nozzle (200 µm) as the electrode, we reformed the hydraulic system that enables the machining of sub-millimeter-sized dimples and channels, which are difficult to achieve with larger nozzles. The machined dimples and channels on TA2 have been characterized using scanning electron microscopy (SEM) and laser scanning confocal microscopy (LSCM) to explore the correlation between the process parameters and EJM performance and compare the effects of the current mode on the EJM of TA2. The main conclusions are summarized as follows:

Fig. 17 SEM images of channels under the pulsed current with different scanning rates: **a** 0.02 mm/s; **b** 0.07 mm/s
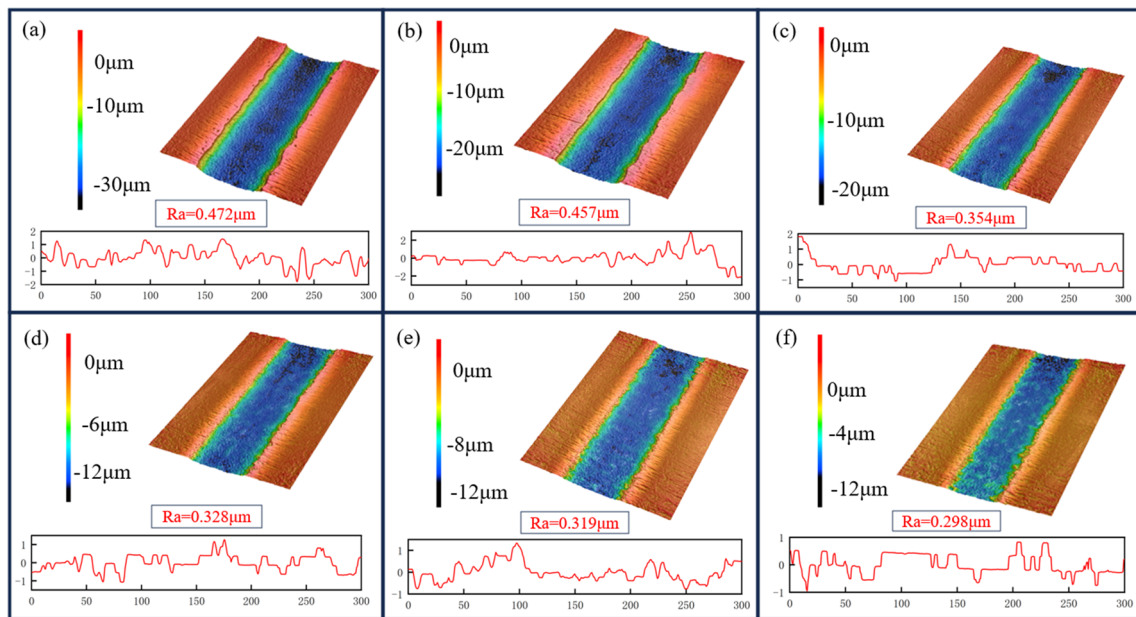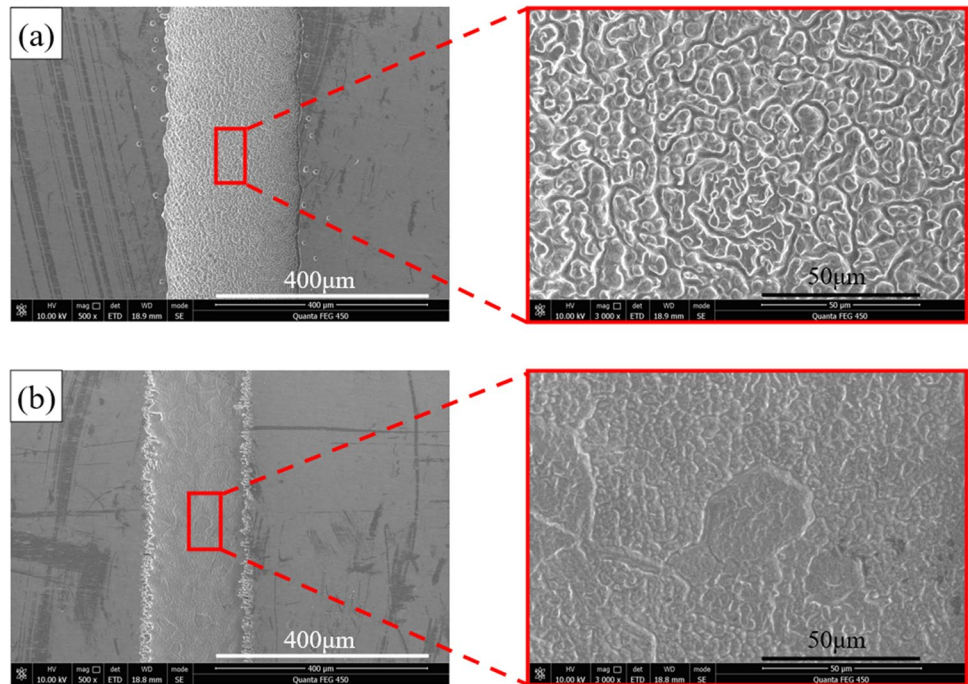

Fig. 18 Depth cloud maps of channels at different scanning rates with the pulsed current of 0.5 duty ratio: **a** 0.02 mm/s; **b** 0.03 mm/s; **c** 0.04 mm/s; **d** 0.05 mm/s; **e** 0.06 mm/s; **f** 0.07 mm/s

1) The experimental results of dimple machining using the EJM technique showed that the depth of dimples machined by pulsed current is greater than that of dimples machined by direct current. Specifically, under the conditions of 100 V and the t_{effv} of 5 s, the depth of dimples machined using pulsed current is approximately 16.007 μm, while that of dimples machined using direct current is 19.256 μm, representing an approximate 20% increase in depth for direct current machining compared to pulsed current. However, the surface finish of the former is worse compared to the latter. These findings suggest that while greater dimple depths can be achieved by applying pulsed currents, this comes at the cost of impaired surface smoothness. The trade-off
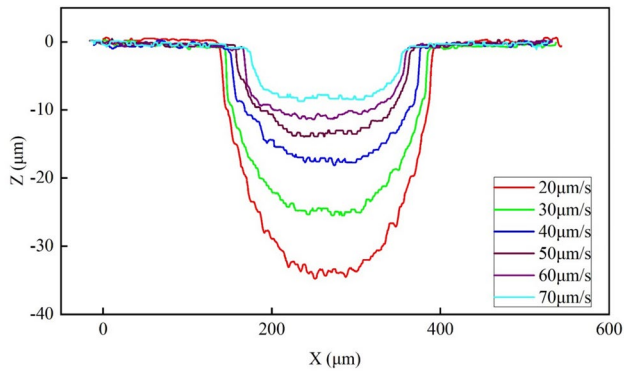
Fig. 19 Cross-sectional views of channels at different scanning rates with the pulsed current of 0.5 duty ratio
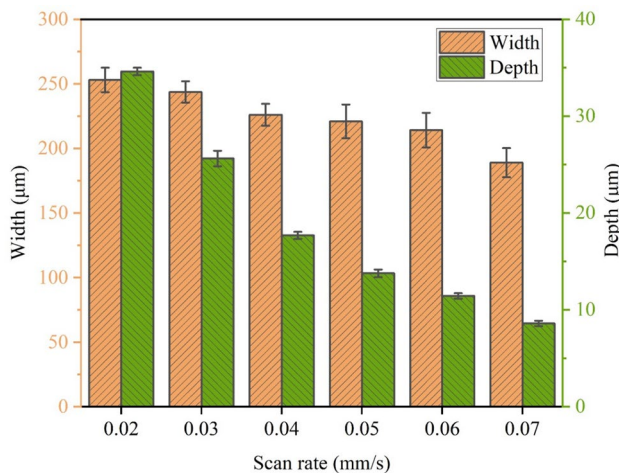

Fig. 20 Histogram of width and depth of channels at different scanning rates with with the pulsed current of 0.5 duty ratio

between depth and surface finish should be considered when selecting the appropriate machining method for a particular application. The experiment indicates that when using direct current, the voltage of 120 V, and the t_{effv} of 10 s, the dimples exhibit higher surface quality.

2) For fabrication of channels, the experimental results show that the direct current mode can achieve better surface roughness on TA2 and the pulsed current mode is more readily available to material removal localization, which implies that using the pulsed current allows for the machining narrower and deeper channels. For example, under a scanning rate of 0.05 mm/s, the depth of channels machined using pulsed current is approximately 13.778 μm, whereas the depth of channels machined using direct current is 26.133 μm, representing an approximate 90% increase in depth for direct current machining compared to pulsed current. Under the conditions of using direct current, a voltage of 140 V,

and the scanning rate of 0.05 mm/s, the machined channel exhibits higher surface quality.

3) EJM with NaCl-EG electrolyte has demonstrated its ability to fabricate submillimetre structures on TA2, implying its proficiency in handling titanium and its alloys. When an appropriate process window is chosen, sharp edges and uniform microstructures can be achieved in both dimples and channels, without dispersed corrosion and flow marks, which always exist in conventional electrochemical machining.

Data availability The authors confirm that material supporting the findings of this work is available within the article. The collected data of this work are not available within the article.

Declarations

Ethical approval Not applicable.

Consent to participate Not applicable.

Consent for publication Not applicable.

Conflict of interest The authors declare no competing interests.

References

1. Tetsui T, Shindo K, Kobayashi S, Takeyama M (2002) A newly developed hot worked TiAl alloy for blades and structural components. Scr Mater 47(6):399–403
2. Li H, Gao C, Wang G, Qu N, Zhu D (2016) A study of electrochemical machining of Ti-6Al-4V in NaNO3 solution. Sci Rep 6(1). https://doi.org/10.1038/srep35013
3. Mwangi JW, Nguyen LT, Bui VD, Berger T, Zeidler H, Schubert A (2019) Nitinol manufacturing and micromachining: a review of processes and their suitability in processing medical-grade nitinol. J Manuf Process 38:355–369
4. Sarilov MY, Myl'nikov VV (2019) Analysis of electrical discharge machining. Tech Phys 64(6):833–838
5. Hung C-H, Chang F-Y (2017) Curve micromachining on the edges of nitinol biliary stent by ultrashort pulses laser. Opt Laser Technol 90:1–6
6. Uppal N, Shiakolas PS (2008) Micromachining characteristics of NiTi based shape memory alloy using femtosecond laser. J Manuf Sci Eng 130(3). https://doi.org/10.1115/1.2936380
7. Cao GQ, Dai YT, Yao L (2011) Study on mechanism of electrochemical micro-machining of titanium alloys. Appl Mech Mater 130–134:2269–2272

8. Qu N, Fang X, Li W, Zeng Y, Zhu D (2013) Wire electrochemical machining with axial electrolyte flushing for titanium alloy. Chin J Aeronaut 26(1):224–229

9. Klocke F, Zeis M, Klink A (2012) Technological and economical capabilities of manufacturing titanium- and nickel-based alloys via electrochemical machining (ECM). Key Eng Mater 504–506:1237–1242

10. Wang F, Zhao J, Lv Y, Fu X, Kang M, Tian Z (2020) Sheet cathode design and experimental study on the electrochemical machining of deep narrow slots in TB6 titanium alloy. Proc Inst Mech Eng Part B: J Eng Manuf 234(4):801–813

11. Liu Y, Qu N (2019) Electrochemical milling of TB6 titanium alloy in NaNO3 solution. J Electrochem Soc 166(2):E35–E49

12. Kozak J (1998) Mathematical models for computer simulation of electrochemical machining processes. J Mater Process Technol 76(1):170–175

13. Kozak J, Chuchro M, Ruszaj A, Karbowski K (2000) The computer aided simulation of electrochemical process with universal spherical electrodes when machining sculptured surfaces. J Mater Process Technol 107(1):283–287

14. Hackert-Oschätzchen M, Paul R, Martin A, Meichsner G, Lehnert N, Schubert A (2015) Study on the dynamic generation of the jet shape in jet electrochemical machining. J Mater Process Technol 223:240–251

15. Schubert A, Hackert-Oschätzchen M, Martin A, Winkler S, Kuhn D, Meichsner G et al (2016) Generation of complex surfaces by superimposed multi-dimensional motion in electrochemical machining. Procedia CIRP 42:384–389

16. Kai S, Sai H, Kunieda M, Izumi H (2012) Study on electrolyte jet cutting. Procedia CIRP 1:627–632

17. Kawanaka T, Kato S, Kunieda M, Murray JW, Clare AT (2014) Selective surface texturing using electrolyte jet machining. Procedia CIRP 13:345–349

18. Speidel A, Mitchell-Smith J, Walsh DA, Hirsch M, Clare A (2016) Electrolyte jet machining of titanium alloys using novel electrolyte solutions. Procedia CIRP 42:367–372

19. Wang M, Qu N (2021) Macro electrolyte jet machining of TC4 titanium alloy using negative-incidence jet form. J Mater Process Technol 294:117148

20. Liu W, Luo Z, Kunieda M (2020) Electrolyte jet machining of Ti1023 titanium alloy using NaCl ethylene glycol-based electrolyte. J Mater Process Technol 283:116731

21. Fushimi K, Habazaki H (2008) Anodic dissolution of titanium in NaCl-containing ethylene glycol. Electrochim Acta 53(8):3371–3376

22. Kawanaka T, Kunieda M (2015) Mirror-like finishing by electrolyte jet machining. CIRP Ann 64(1):237–240

23. Rosenkranz C, Lohrengel MM, Schultze JW (2005) The surface structure during pulsed ECM of iron in NaNO3. Electrochim Acta 50(10):2009–2016